
Article:
Zhang, W. Q., Andreyev, A. N. orcid.org/0000-0003-2828-0262, Liu, Z. et al. (39 more authors) (2022) Identification of excited states in 188Bi and 188Po. Phys. Rev. C. 024317. ISSN 2469-9993

https://doi.org/10.1103/PhysRevC.106.024317

Identification of excited states in ^{188}Bi and ^{188}Po

W. Q. Zhang,[1,2] A. N. Andreyev,[3,4,*] Z. Liu,[1,2,†] D. Seweryniak,[5] H. Huang,[1,2] Z. H. Li,[6] J. G. Li,[1] C. Y. Guo,[6] A. E. Barzakh,[7] P. Van Duppen,[8] M. Al Monthery,[3] B. Andel,[8,9] S. Antalic,[9] M. Block,[10,11,12] A. Bronis,[9] M. P. Carpenter,[5] P. Copp,[5] J. G. Cubiss,[3] B. Ding,[1,2] D. T. Doherty,[13] Z. Favier,[14] F. Giacoppo,[10,11] T. H. Huang,[1,2] B. Kindler,[11] F. G. Kondev,[5] T. Lauritsen,[5] G. S. Li,[1,2] B. Lommel,[11] H. Y. Lu,[1,2] P. Mošať,[9] Y. F. Niu,[15] C. Raison,[3] W. Reviol,[5] G. Savard,[5] S. Stolze,[5] G. L. Wilson,[16] H. Y. Wu,[6] Z. H. Wang,[15] F. R. Xu,[6] X. H. Yu,[1,2] Q. B. Zeng,[1,2] and X. H. Zhou[1,2]

[1]*Institute of Modern Physics, Chinese Academy of Sciences, Lanzhou 730000, China*
[2]*University of Chinese Academy of Sciences, Beijing 100049, China*
[3]*Department of Physics, University of York, York YO10 5DD, United Kingdom*
[4]*Advanced Science Research Center (ASRC), Japan Atomic Energy Agency, Tokai-mura, Japan*
[5]*Physics Division, Argonne National Laboratory, Argonne, Illinois 60439, USA*
[6]*State Key Laboratory of Nuclear Physics and Technology, School of Physics, Peking University, Beijing 100871, China*
[7]*Petersburg Nuclear Physics Institute, NRC Kurchatov Institute, 188300 Gatchina, Russia*
[8]*KU Leuven, Instituut voor Kern- en Stralingsfysica, 3001 Leuven, Belgium*
[9]*Department of Nuclear Physics and Biophysics, Comenius University in Bratislava, 84248 Bratislava, Slovakia*
[10]*Helmholtz-Institut Mainz, Mainz 55128, Germany*
[11]*GSI Helmholtzzentrum für Schwerionenforschung Darmstadt, Darmstadt, 64291, Germany*
[12]*Johannes-Gutenberg Universität, Mainz 55099, Germany*
[13]*Department of Physics, University of Surrey, Guildford GU2 7XH, United Kingdom*
[14]*Irfu, CEA, Université Paris-Saclay, F-91191 Gif-sur-Yvette, France*
[15]*Lanzhou University, Lanzhou 730000, China*
[16]*Department of Physics and Astronomy, Louisiana State University, Baton Rouge, Louisiana 70803, USA*

(Received 12 May 2022; accepted 1 August 2022; published 17 August 2022)

The neutron-deficient ^{188}Bi and ^{188}Po isotopes have been studied by γ-ray spectroscopy using the recoil-decay tagging technique with the Argonne Gas-Filled Analyzer. A new 0.25(5)-μs isomeric state and a prompt cascade formed by 319-, 366-, and 462-keV γ rays have been established on top of the (10^-) α-decaying isomer in ^{188}Bi. The first excited (2^+) state in ^{188}Po was identified, its excitation energy of 242(2) keV continues the nearly constant trend for the first 2^+ states in ^{190,192,194}Po. The state is most likely a member of a prolate rotational band built on the ground state, albeit mixing with other coexisting configurations cannot be excluded. The new results obtained in the present work provide new information to shape coexistence in bismuth and polonium isotopes near the neutron midshell at $N = 104$. In this mass region, a reduction in the prompt γ-ray yield obtained with recoil decay tagging was observed for a few nuclides, and the possible reasons are presented.

DOI: 10.1103/PhysRevC.106.024317

I. INTRODUCTION

Shape coexistence phenomena at low excitation energy are extensively established, both experimentally and theoretically, across the nuclear chart [1,2]. In particular, abundant shape coexistence cases have been known around the neutron midshell at $N = 104$, where the number of valence neutrons in the $N = 82$–126 neutron valence space is maximized, amplifying the proton-neutron correlations. For the $Z \leqslant 82$ region around $N \approx 104$, relatively comprehensive experimental data exist [3,4]. In contrast, as the fusion-fission channel becomes dominant for compound nuclei with $Z > 82$, the lightest bismuth and polonium isotopes in the vicinity of $N \approx 104$ are scarcely studied. Importantly, shape coexistence is expected in the ^{188}Bi and ^{188}Po isotopes, which are the main subject of the present investigation.

A particular motivation for our study was given by the recent laser-spectroscopy work on light ^{187,188,189,191}Bi ($Z = 83$) isotopes at ISOLDE-CERN [5]. There, a large shape staggering was found, manifested by a drastic increase of the mean-square charge radius for ^{188}Bi^g ($N = 105$) in comparison with the neighboring ^{187g,189g}Bi ($N = 104$, 106) and with ^{188}Bi^m. The magnitude of this effect is comparable with the well known shape staggering in $^{181-185}$Hg and it starts at the same neutron number, $N = 105$ [6,7].

Two predominantly α-decaying states are known in ^{188}Bi: the $1^{(+)}$ ground state (gs) based on the presumed $\pi 1/2^-[530]f_{7/2} \otimes \nu 1/2^-[521]p_{3/2}$ configuration [5,8], and the (10^-) isomer from the $\pi h_{9/2} \otimes \nu i_{13/2}$ coupling [9]. Based

*andrei.andreyev@york.ac.uk
†liuzhong@impcas.ac.cn

on laser-spectroscopy studies [5], the $1^{(+)}_{gs}$ was found to be strongly prolate deformed with $\beta = +0.25(7)$, whereas the (10^-) isomer is nearly spherical. The half-life and energy of the most intense α decay evaluated previously for the $1^{(+)}_{gs}$ of ^{188}Bi are 60(3) ms and 6992(5) keV, respectively, and for the (10^-) isomer 265(10) ms and 6813(5) keV [9,10]. Furthermore, several excited states above ^{188}Bi^{g,m} were identified in α-decay investigations of ^{192m1,m2}At [11]. The isomer versus gs shape staggering in ^{188}Bi can be further studied via the observation and characterization of excited states on top of ^{188}Bi^{g,m}, whereby very different band structures could be expected.

The earlier laser-spectroscopy studies have established that the ground states of even-mass $^{200-210}$Po ($Z = 84$) isotopes are nearly spherical [12], which was also confirmed by in-beam γ-ray spectroscopy of their low-lying excited states [4]. However, an abrupt drop and a parabolic behavior as a function of neutron number of the yrast and near-yrast state energies was observed in in-beam studies of $^{190-198}$Po approaching $N = 104$ [13–18]; see Fig. 4 in Ref. [18]. Two different approaches were invoked in the 1990s for the interpretation of this observation: an anharmonic quadrupole vibrator picture [15,17,19,20] versus the intruder/shape coexistence framework and configuration mixing [13,14,18,21–26]. The latter interpretation was strongly supported down to ^{192}Po ($N = 108$) [27–29] by laser-spectroscopy experiments in the first decade of 21st century, whereby a surprisingly sudden and early departure from sphericity was observed for the ground states of $^{192-198}$Po isotopes. This inference is further supported by the α-decay fine structure pattern in $^{186-198}$Po, combined with potential-energy surface (PES) calculations, whereby a prolate gs was proposed for ^{186,188}Po [30–32].

In the present study, the first in-beam spectroscopy of ^{188}Bi and ^{188}Po was performed at the Argonne Gas-Filled Analyzer (AGFA) [33]. For ^{188}Po, only the 0^+_{gs} was known from α-decay studies [30,34]. The half-life and the energy of the most intense α decay evaluated previously for ^{188}Po are 0.27(3) ms and 7911(13) keV, respectively. The data for ^{187}Pb and for ^{183}Hg from the same experiment were previously presented in Refs. [35,36].

II. EXPERIMENTAL SETUP

The ^{188}Bi and ^{188}Po nuclei were produced via the $p3n$ and $4n$ evaporation channels of the complete-fusion reaction ^{50}Cr + ^{142}Nd → ^{192}Po*, respectively. A 255-MeV ^{50}Cr beam with a typical intensity of 7 p nA was delivered by the ATLAS superconducting linear accelerator, at Argonne National Laboratory (ANL). Targets with a thickness of 700 μg/cm^2 were prepared from the chemical compound ^{142}NdF$_3$ with an isotopic enrichment of ≈99.8% for neodymium. Four target sectors were mounted on a rotating wheel, and the beam was wobbled ±2.5 mm vertically across the target by a magnetic steerer to avoid the target melting. During a one-week experiment, the effective beam-on-target time is ≈130 hours.

Evaporation residues (EVRs) were separated from the primary beam by AGFA filled with ≈0.65 mbar of helium gas, and transported to the focal-plane detector system. A position-sensitive parallel grid avalanche counter (PGAC), located at the exit from AGFA, provided time of arrival and energy-loss signals of EVRs. The recoiling nuclei were subsequently implanted into a 64 mm × 64 mm, 300 μm thick double-sided silicon strip detector (DSSD) with 160 × 160 pixels located 40 cm behind the PGAC. The DSSD detected the implantation of EVRs and their subsequent decays, and allowed application of the standard temporal and spatial recoil-decay correlation technique. The typical count rates is ≈300 Hz for the implantation in the DSSD. The typical full width at half maximum (FWHM) of energy resolution for the DSSD was ≈30 keV for 5.4–7.2 MeV α particles. A Sibox, composed of eight single-sided silicon strip detectors mounted perpendicularly on the sides of the DSSD, was used to register the escaping α particles. The total full-energy α-particle detection efficiency of the DSSD + Sibox was measured to be ≈75%.

Four clover high-purity germanium (HPGe) detectors (the X-Array) [37] consisting of four crystals each, surrounded the DSSD chamber and were used for delayed EVR-γ and prompt α-γ coincidence measurements. The typical energy resolution and detection efficiency for the X-Array were ≈3.4 keV (FWHM) and ≈16% for γ-ray energies around 250 keV.

Prompt γ rays at the target position were detected by the Gammasphere (GS) array [38] with 64 large-volume Compton-suppressed Ge detectors. A time window from −100 to 100 ns was used for prompt $\gamma\gamma$ coincidences in the GS. The typical energy resolution and detection efficiency for GS were ≈3.5 keV (FWHM) and ≈12% for γ-ray energies around 300 keV. The recoil-decay tagging (RDT) technique [39,40] was used to provide an unambiguous γ-ray assignment to a specific nuclide.

III. DATA ANALYSES

A. The calibration of the DSSD and DSSD + Sibox energy spectra

Figure 1(a) provides a part of the α-decay spectrum registered in the DSSD within 5 s following the EVRs implantation. It shows several peaks corresponding to the α decays of ^{183}Hg [5904(5) keV], ^{184}Hg [5539(5) keV], ^{185}Hg [5653(5) keV], ^{186}Pb [6331(6) keV], ^{187}Pb^m [6077(7) keV], ^{188}Bi^m [6813(5) keV], ^{188}Bi^g [6992(5) keV], and ^{189}Bi [6670.9(22) keV], evaluated in Refs. [10,42], which were used for the DSSD calibration. With this calibration, we reproduce the energies of all peaks, shown in Fig. 1(a), within 1–3 keV, and the measured energies will be used in the text.

The energy spectrum of escaping α particles could be reconstructed by adding the energy depositions in the DSSD and Sibox, after the Sibox energy calibration was performed. The energy deposition of the escaping α particles in the dead layers of the Si detectors (DSSD and Sibox) has been corrected in the calibration. The spectrum is shown in Fig. 1(b), with a typical energy resolution of ≈120 keV (FWHM) in the 6.5–7.2 MeV α-energy range. Despite a relatively poor energy resolution in

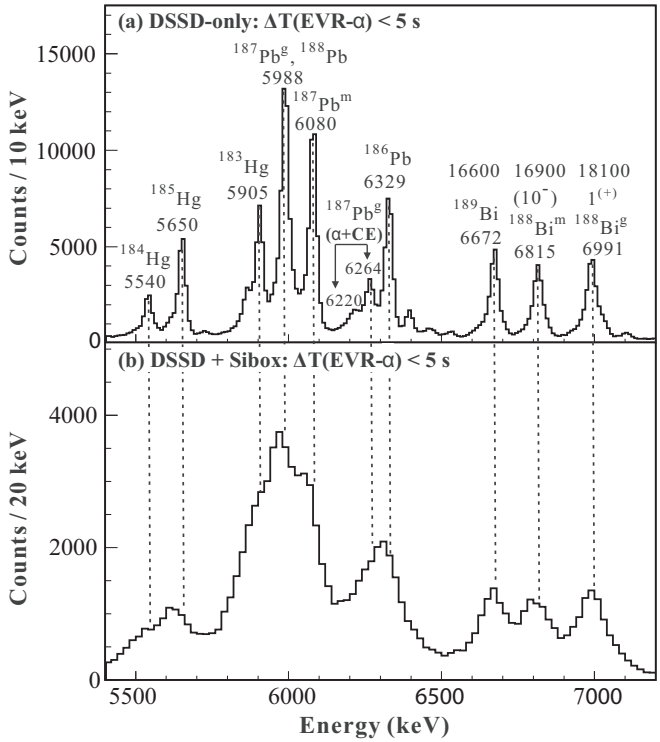

FIG. 1. (a) A part of the energy spectrum for α particles, registered in the DSSD only, following EVRs' implantation within 5 s. (b) The same, but for escaping α particles, being the sum of α-particle energies measured in the DSSD and Sibox. The vertical dashed lines show the correspondence of the peaks in the two spectra. The approximate numbers of counts (DSSD only) for the full-energy α peaks of ^{188}Bi^{g,m} and ^{189}Bi are shown above each peak. The structure at 6220 to 6264 keV corresponds to the partial or full energy summing in the DSSD of the 6194-keV α decay of ^{187}Pb^{g} and ≈54–64 keV L/M-shell conversion electrons (CEs) resulting from the strong conversion of the known coincident 67-keV $E2$ transition [41].

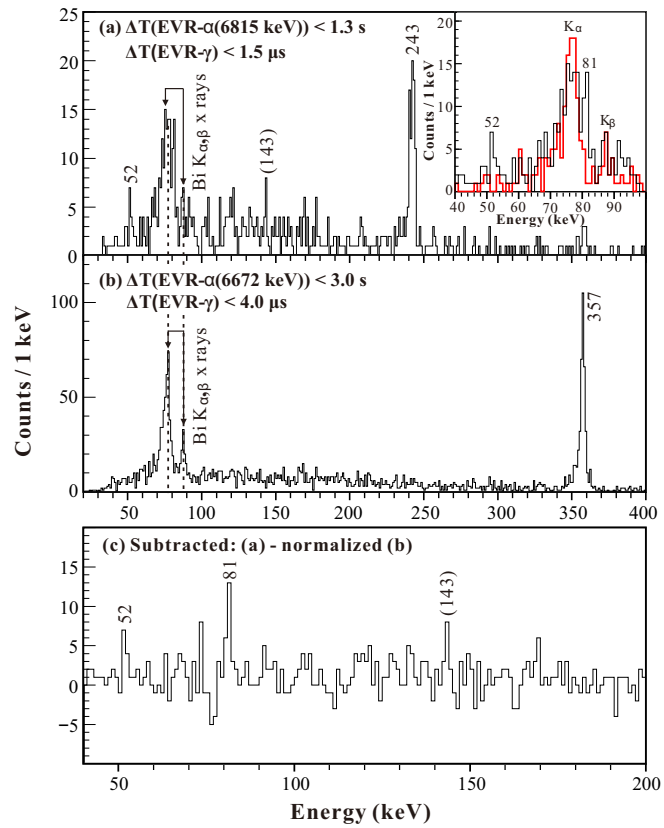

FIG. 2. (a) The delayed γ-ray energy spectrum obtained by tagging on the combined statistics of the 6815-keV α decay of ^{188}Bi^{m} in DSSD only. (b) The same, but gated by the 6672-keV α decay of ^{189}Bi. The tagging time intervals are shown in the panel titles. The inset in (a) shows the overlay of the zoomed-in spectra from panels (a) (in black) and (b) (in red), after normalization to the same number of Bi K_α x rays as seen in panel (a). (c) The difference of the spectra from panels (a) and (b) after normalization to the same number of Bi K_α x-ray counts as seen in (a).

the reconstructed spectrum, a clear correspondence between the peaks in Figs. 1(a) and 1(b) can be seen, which allowed us to also use the DSSD + Sibox data for analysis. An energy window of ±35 keV was used when gating on the DSSD-only data, and ±90 keV for the DSSD + Sibox events.

B. Excited states in ^{188}Bi^{m,g}

The peak at 6815(4) keV in Fig. 1(a) corresponds to the 6813(5)-keV α decay of the (10^-) ^{188}Bi^{m}, while the peak at 6991(4) keV is due to the α decay of the $1^{(+)}_{gs}$ of ^{188}Bi [9,10]. To search for the delayed and prompt γ rays in ^{188}Bi, both the DSSD-only and DSSD + Sibox data were used.

1. A new isomeric state above ^{188}Bi^{m}

Figure 2(a) shows the energy spectrum of the delayed γ rays registered in the X-Array, within 1.5 μs of the implantation of EVRs and followed by the 6815-keV peak of ^{188}Bi^{m} within the time interval of ΔT(EVR-α) < 1.3 s. A 243(1)-keV γ ray was assigned to the deexcitation of a new isomeric state above ^{188}Bi^{m}. Apart from the 243-keV γ ray and Bi $K_{\alpha,\beta}$ x rays, several peaks, i.e., at 52(1) and 81(1) keV [see the inset in Fig. 2 (a)], and tentatively at 143(1) keV, are also seen in the delayed spectrum. These γ rays will also be attributed to the deexcitation of the same isomer, as discussed below.

Figure 2(b) shows an X-Array spectrum with a gate on the 6672-keV decay of ^{189}Bi, which demonstrates the presence of the known 357-keV isomeric γ ray from the $(13/2^+)$ isomer. The deduced half-life of this isomer is 0.82(5) μs [see Fig. 3 (b)], and is in agreement with the previously reported value of 0.88(5) μs [43]. The inset of Fig. 2 (a) shows the overlay of the spectra from panels (a) and (b), when the latter spectrum is normalized on the same number of Bi $K_{\alpha,\beta}$ x-ray events as seen in panel (a). This overlay clearly confirms the presence of the 52- and 81-keV γ rays, which is also seen in the subtracted spectrum in Fig. 2 (c), under the same normalization conditions as in the inset. The 143-keV peak is also tentatively seen in the subtracted spectrum.

By fitting the time distribution ΔT(EVR − γ(243 keV)), the half-life of the isomer is determined to be 0.25(5) μs,

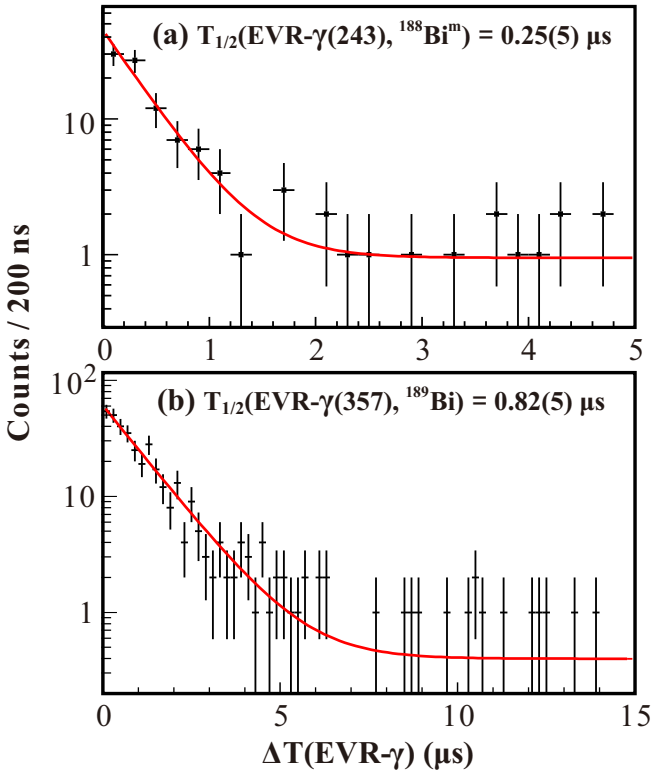

FIG. 3. (a) The time difference ΔT(EVR − γ(243 keV, ^{188}Bi^{m})), and the associated fit by an exponential function with a constant background using maximum likelihood method. (b) The same, but for the time difference ΔT(EVR − γ(357 keV, ^{189g}Bi)).

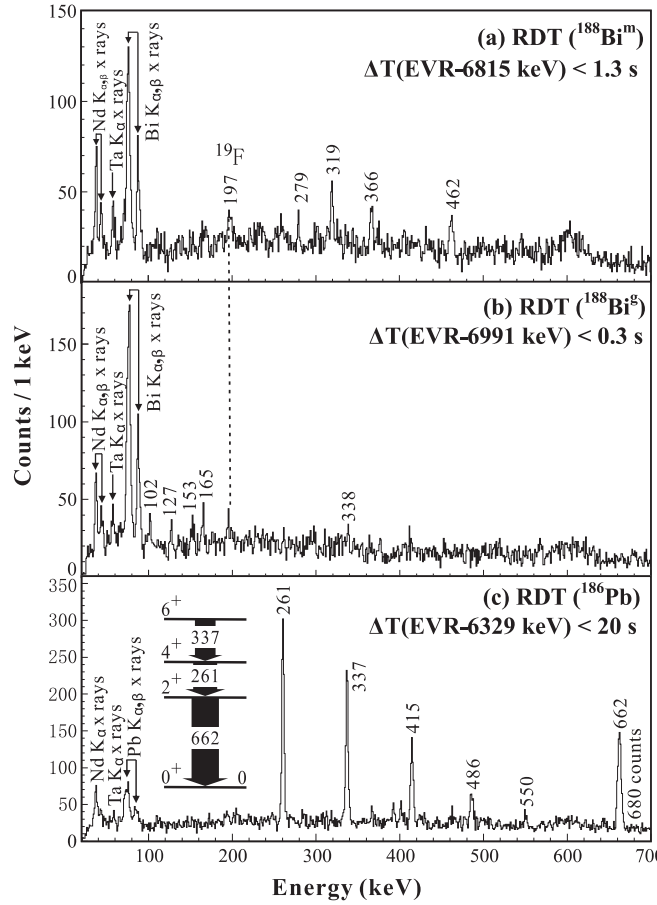

FIG. 4. (a) The combined prompt γ-ray energy spectrum in GS obtained by tagging on the 6815-keV decay of ^{188}Bi^{m} in DSSD only and DSSD + Sibox. (b) The same, but gated by the 6991-keV peak of ^{188}Bi^{g}. (c) The same, but for the 6329-keV peak of ^{186}Pb and after normalizing to approximately the same number of α decays as for ^{188}Bi^{g,m} in panels (a) and (b). The partial level scheme of yrast states up to 6^{+} in ^{186}Pb and the number of the 662-keV γ rays are also shown in panel (c). The tagging time intervals are given in the panel titles. The $K_{\alpha,\beta}$ x rays from element Nd in the target and the K_{α} x ray from Ta absorbers in front of the Ge detectors are also present. The 197-keV line is from the Coulomb excitation of ^{19}F in the target.

as shown in Fig. 3(a). The half-life of the combined $K_{\alpha,\beta}$ x rays and 52- and 81-keV γ rays is 0.35(10) μs, which is consistent within the uncertainty with the half-life of 0.25(5) μs of the 243-keV γ ray, thus we assume that all these γ rays originate from the same isomer. We use the half-life of the 243-keV decay as the final value, as the time resolution of the X-Array is worse at lower energies. Due to the lack of statistics, we cannot prove any $\gamma\gamma$ coincidences between the 52-, 81-, 143-, and 243-keV γ rays. As both the 143- and 243-keV transitions can produce $K_{\alpha,\beta}$ x rays, their internal conversion coefficients and multipolarities cannot be deduced. If the 143-keV transition would not exist, then a conversion coefficient of $\alpha_K(243\ \text{keV}) = 1.9(4)$ could be derived, if one assigns all observed Bi $K_{\alpha,\beta}$ x rays to the conversion of the 243-keV transition.[1] However, we prefer to refrain from further evaluation of a possible multipolarity for this transition in view of the unclear level scheme.

2. *RDT analysis for* ^{188}Bi^{m}

To search for prompt γ-ray transitions of a specific nuclide detected by GS, the RDT method was used. Figure 4 shows prompt γ-ray spectra for ^{188}Bi^{m} [Fig. 4(a)] and ^{188}Bi^{g} [Fig. 4(b)], and to demonstrate contrast in γ-ray intensities it also shows the spectrum for ^{186}Pb [Fig. 4(c)]. The recoil-gated, α-tagged γ-ray energy spectrum of ^{188}Bi^{m} is shown in Fig. 4(a). The presence of weak γ lines at 279(1), 319(1), 366(1) and 462(1) keV in comparison with strong Bi $K_{\alpha,\beta}$ x rays suggests the dominant internal conversion of γ transitions on top of ^{188}Bi^{m}. The RDT spectrum for ^{186}Pb in Fig. 4(c) was obtained by tagging on the 6329-keV α line, normalized to the approximately same number of α decays of ^{188}Bi^{g,m}. A prominent difference in γ-ray intensities between the two spectra can be clearly seen, with strong known yrast γ-ray peaks and weak Pb $K_{\alpha,\beta}$ x rays for ^{186}Pb. This difference [also for ^{188}Bi^{g}, shown in Fig. 4(b)] will be discussed in Sec. IV D in more detail.

The representative $\gamma\gamma$ coincidence spectra from RDT of ^{188}Bi^{m} are given in Fig. 5; they confirm the mutual co-

[1]The 52- and 81-keV γ rays are below the Bi K-shell electron binding energy of 90.526 keV.

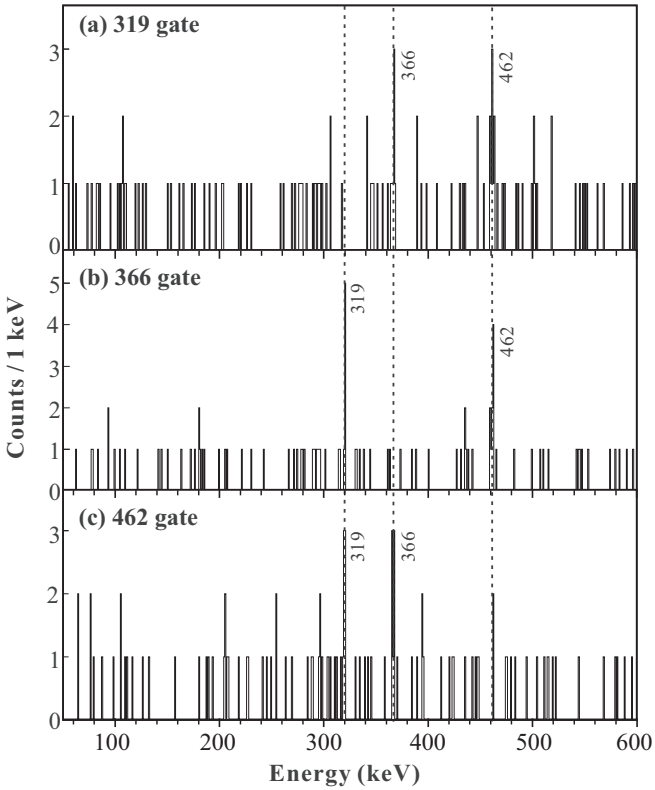

FIG. 5. (a)–(c) Recoil-gated $\gamma\gamma$ coincidence energy spectra tagged with the 6815-keV α decay of ^{188}Bi^{m}. The gating γ rays are indicated in the panel titles.

incidences between the 319-, 366-, and 462-keV γ rays. Therefore, these transitions form a prompt cascade. The intensities of the three γ rays are the same within uncertainties, thus their relative ordering could not be established assuming comparable conversion coefficients. Furthermore, an isomer-decay tagging (IDT) analysis was tried by tagging on the γ rays below the 0.25(5)-μs isomer, but the IDT spectrum with no obvious peaks cannot prove or disprove whether the cascade is built on the isomer.

Based on the data presented in this section, we propose the level scheme for ^{188}Bi^{m} as shown in the middle of Fig. 6. The relative positions of the 0.25(5)-μs isomer and the prompt cascade, and their intensities relative to the 6815-keV α decay, will be further discussed in Sec. IV A.

3. *RDT analysis for* ^{188}Bi^{g}

Figure 4(b) shows the prompt γ-ray energy spectrum obtained by tagging on the 6991-keV peak of ^{188}Bi^{g}. Similar to the γ-ray energy spectrum of ^{188}Bi^{m} obtained employing the RDT technique, the Bi $K_{\alpha,\beta}$ x rays are also strongest in Fig. 4(b), even ≈30% stronger relative to ^{188}Bi^{m} [Fig. 4(a)] after normalizing to the same number of α decays. Based on the RDT analysis, we identified a number of new transitions at 102(1), 127(1), 153(1), and 165(1) keV, and tentatively at 338(1) keV. All of these transitions belong to ^{188}Bi^{g} as they are not present in the ^{188}Bi^{m} RDT spectrum, but due to the absence of $\gamma\gamma$ coincidences they could only be placed schematically in the level scheme in Fig. 6.

In the α-decay study of ^{192}At → ^{188}Bi, 165(1)-keV and 188(1)-keV transitions were proposed as feeding directly to ^{188}Bi^{m} [11]. However, we do not observe these γ lines in the RDT spectrum for ^{188}Bi^{m} [Fig. 4(a)]; meanwhile a 165(1)-keV γ line is present in the RDT spectrum for ^{188}Bi^{g} [Fig. 4 (b)]. It is unclear from the previous and present data if there are two

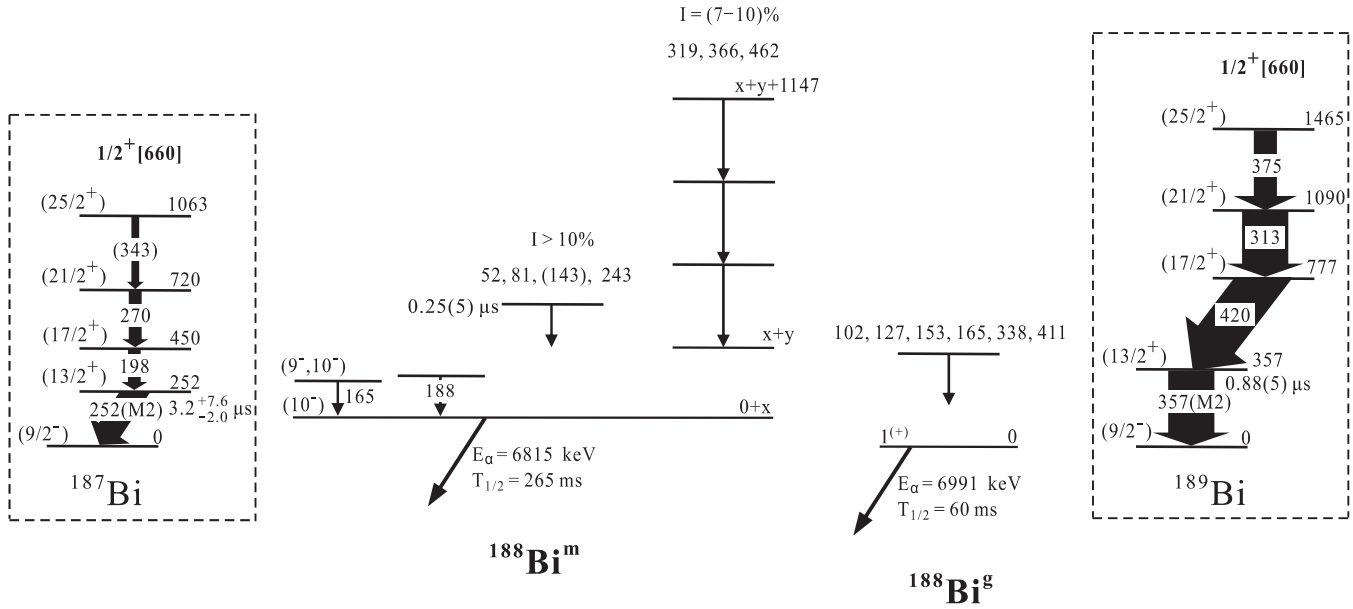

FIG. 6. Proposed level scheme for ^{188}Bi^{g,m}. The excitation energy of 153(30) keV for ^{188}Bi^{m} is from Ref. [44]. The 165- and 188-keV transitions feeding the isomeric (10^{-}) ^{188}Bi^{m} are taken from Ref. [11]. The symbol "I" above the levels represents intensities for the isomer and cascade relative to the 6815-keV α decay. The panels to the leftmost and rightmost show partial level schemes for ^{187,189}Bi [45].

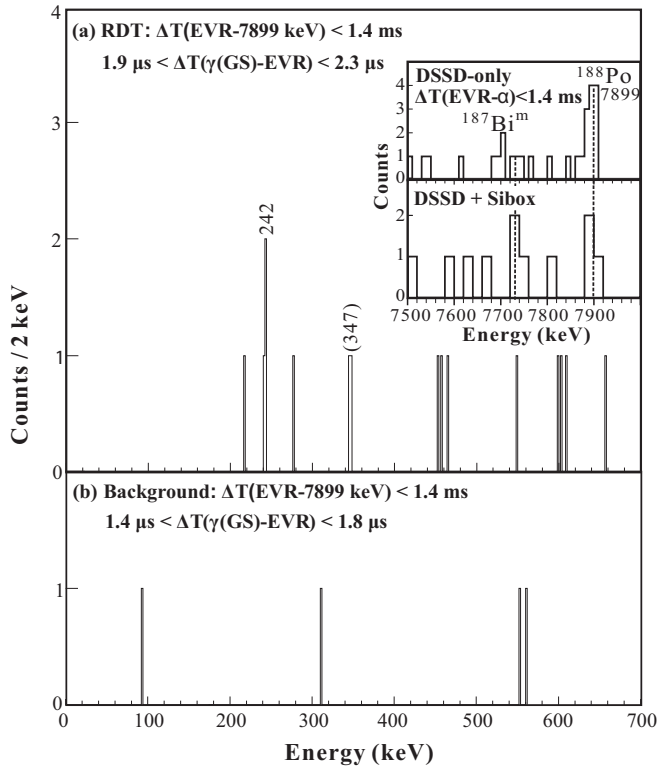

FIG. 7. (a) The prompt RDT γ-ray energy spectrum in GS obtained by tagging on the 7899-keV α decay of ^{188}Po; see main text for details. (b) The corresponding background RDT spectrum gated by the random time window between the EVRs and the γ rays registered in GS, with the same condition on α decay. The tagging time windows for the RDT spectrum and background spectrum are indicated in the panel titles. The top and bottom panels in the inset show parts of the corresponding α-decay spectra registered in the DSSD only and the DSSD + Sibox, respectively.

165-keV transitions present in ^{188}Bi or if they represent the same decay.

We note that a search for μs isomers was also performed for ^{188}Bi^{g}, but no candidates for isomeric transitions were found.

C. The first (2$^+$) state in ^{188}Po

Parts of the α-particle energy spectra relevant to ^{188}Po as measured in the DSSD only and DSSD + Sibox within $\Delta T(\mathrm{EVR}-\alpha) < 1.4$ ms are shown in top and bottom panels of the inset in Fig. 7(a). The peak at 7899(16) keV corresponds to the 7911(13)-keV α decay of ^{188}Po [30,46]. Similarly to ^{188}Bi, both the DSSD only and DSSD + Sibox data were used for the RDT analysis of ^{188}Po. Figure 7(a) shows the prompt γ-ray energy spectrum obtained by tagging on the 7899-keV decay within the time window of $1.9 < \Delta T(\gamma(\mathrm{GS}) - \mathrm{EVR}) < 2.3$ μs. This time window covers the peak of prompt coincidences in the GS gated by recoil registered in the DSSD.

A 242(2)-keV peak with three counts is seen in Fig. 7(a). The small number of events requires a few considerations about its authenticity. By using the same significance analysis method as in Ref. [45], we estimate the probability of the 242-keV peak being random fluctuations of the background to be less than 0.3%. In addition, Fig. 7(b) shows the background spectrum gated by the ^{188}Po α decay within the time window of $1.4 < \Delta T(\gamma(\mathrm{GS}) - \mathrm{EVR}) < 1.8$ μs. The length of this random time window is the same as that of the real RDT correlation time window. The fact that only single-count "peaks" are present in Fig. 7(b) provides a further evidence for the presence of the 242-keV peak. As will be shown in Sec. IV C, based on the systematics of excited states in even-even polonium isotopes, the 242-keV γ ray is assigned as proceeding from the first excited (2$^+$) state in ^{188}Po. Besides the 242-keV peak, a two-counts peak at 347(3) keV could be tentatively attributed to ^{188}Po, but we refrain from making this assignment.

IV. DISCUSSION

A. ^{188}Bi^{m}

To understand the strong presence of Bi $K_{\alpha,\beta}$ x rays in Fig. 4(a) we considered the intensity balance between the 279-, 319-, 366-, and 462-keV γ rays on the one hand, and the $K_{\alpha,\beta}$ x rays on the other hand. Due to their prompt nature, the possible multipolarities for these transitions should be limited to $E1$, $M1$, or $E2$. We note that the K-conversion coefficients for transitions with $M1$ multipolarity are the largest, e.g., $\alpha_K(279\ \mathrm{keV}, M1) = 0.462$, $\alpha_K(279\ \mathrm{keV}, E1) = 0.029$, and $\alpha_K(279\ \mathrm{keV}, E2) = 0.078$ [47]. By considering the K conversion with either $E1$ or $M1$ multipolarity, we can account only for 2%($E1$)–25%($M1$) of the $K_{\alpha,\beta}$ x-ray intensity observed in Fig. 4(a). The higher number of observed $K_{\alpha,\beta}$ x rays suggests that some additional prompt transitions with E_γ above the Bi K-shell electron binding energy of 90.526 keV should be present in ^{188}Bi^{m}, but are not seen due to strong internal conversion.

Furthermore, a range of (7–10)% for the intensity of the prompt 319-366-462-keV cascade relative to the 6815-keV α decay was deduced, by assuming either $E1$, $E2$, or $M1$ multipolarity for these transitions.

To determine the intensity of the isomeric deexcitation path, Fig. 8 shows the intensity balance, relative to the 6815-keV α decay, for the 52-, 81-, 143-, and 243-keV transitions originating from the 0.25(5)-μs isomer above ^{188}Bi^{m}. As shown in Fig. 8, a range of possible multipolarities is considered for each case, while the higher multipolarities are excluded due to too long expected half-lives or due to their high conversion coefficients leading to much higher transition intensities relative to the α decay. For example, assuming $E2$ for the 52-keV transition would result in 1450% for its intensity. Similarly, the Weisskopf half-life [48] of a 243-keV $E3$ transition would be $\approx$4 ms, far exceeding the measured half-life of the isomer.

Based on the intensity balance in Fig. 8, several level-scheme scenarios for the isomer are possible. However, due to lack of $\gamma\gamma$ coincidences we prefer not to speculate on the specific isomeric deexcitation path, and thus the 52-, 81-, 143-, and 243-keV transitions could only be placed schematically in the level scheme in Fig. 6. Importantly, irrespective

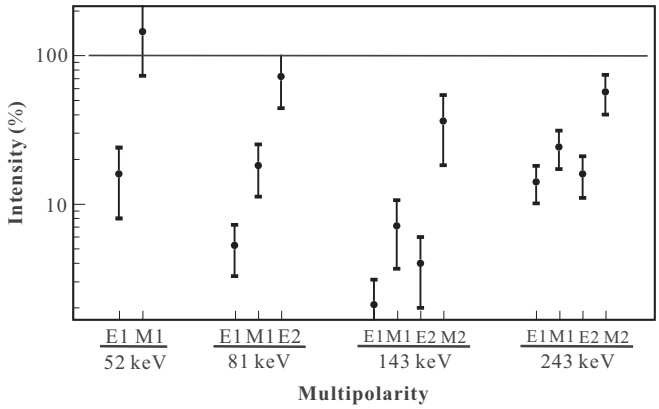

FIG. 8. Intensities are given for the isomeric 52-, 81-, 143-, and 243-keV γ rays relative to the number of 6815-keV α-decays of ^{188}Bi^m, which is taken as 100% and shown by a solid horizontal line in the figure. The values are corrected for γ-ray efficiency and for respective internal conversion for each possible multipolarity considered.

of the level scheme of the isomer, a lower limit of 10% can be deduced for the intensity of the deexcitation path through the isomer. This value is determined by the lowest possible $E1$ multipolarity for the 52-keV decay.

Based on the deduced intensity values we cannot establish whether the prompt cascade feeds to the 0.25(5)-μs isomer or directly to the α-decaying isomer ^{188}Bi^m, which is why it is presently shown as "floating" relative to ^{188}Bi^m in Fig. 6.

To get insight into the possible configurations in the odd-odd ^{188}Bi, the systematics of the lowest single-proton states in the odd-mass Bi isotopes $^{187-195}$Bi [10], are shown in Fig. 9. For the convenience of the discussion, we also added the partial level schemes for neighboring ^{187,189}Bi in Fig. 6. Figure 9

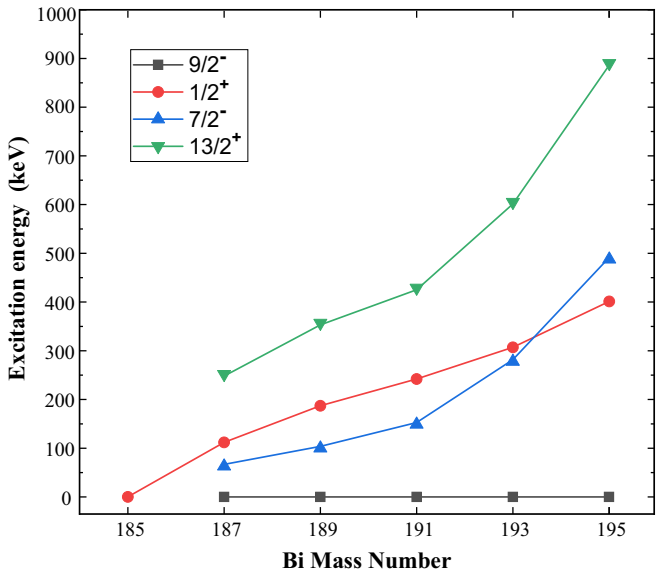

FIG. 9. The excitation energies for the lowest single-proton states in the odd-mass Bi isotopes, close to ^{188}Bi. The data are taken from Ref. [10].

demonstrates a strong downward trend in excitation energy of the $1/2^+$, $7/2^-$, and $13/2^+$ states, relative to the $9/2^-_{gs}$, when approaching the neutron midshell at $N = 104$ (^{187}Bi). In both ^{187,189}Bi these four states are actually the lowest-lying levels, with all of them observed within ≈350 keV. Furthermore, the $13/2^+$ states are the μs-order isomers deexcited by the $13/2^+ \rightarrow 9/2^- M2$ transitions in $^{187-195}$Bi [43]. Therefore in ^{188}Bi one could expect a coupling of, e.g., an $i_{13/2}$ neutron close to the Fermi surface around $N = 104$ to a proton in those low-lying orbitals, producing a variety of p-n multiplet states at low energy. These states most probably deexcite by low-energy transitions and some of them might become isomeric, as is known in many odd-odd nuclei in this region [49]. But in contrast to the odd-mass cases, where only very few transitions are possible for the $13/2^+$ isomers, e.g., $13/2^+ \rightarrow 9/2^-$ or $13/2^+ \rightarrow 7/2^-$, a more complex deexcitation path may arise in ^{188}Bi^m due to the presence of several multiplet states and prompt $M1$ and/or $E2$ transitions between them. The 0.25(5)-μs isomer in ^{188}Bi^m deexciting by a few transitions, as proposed in this study, could represent this scenario.

The prompt cascade on top of ^{188}Bi^m could be similar to the decoupled prolate rotational bands based on the presumable $\pi 1/2^+[660]i_{13/2}$ Nilsson orbital in ^{187,189}Bi [45], e.g., the 462-319-366-keV sequence in ^{188}Bi^m versus the 420-313-375-keV band in ^{189}Bi, as shown in Fig. 6. Therefore, tentatively, this cascade could be a candidate for a decoupled prolate rotational band in ^{188}Bi.

B. Tentative confirmation of strong deformation of ^{188}Bi^g

The RDT spectrum for ^{188}Bi^g in Fig. 4(b) is clearly different from that for ^{188}Bi^m in Fig. 4(a), with only weak evidence for higher-energy γ rays above 200 keV and with the presence of several low-energy γ rays (102, 127, 153, and 165 keV) and stronger Bi $K_{\alpha,\beta}$ x rays. These γ rays are shown schematically in Fig. 6.

A strongly deformed $1^{(+)}$ state with $\beta = +0.25(7)$ was proposed for ^{188}Bi^g from the ISOLDE laser-spectroscopy study [5], the observed γ-ray and $K_{\alpha,\beta}$ patterns associated with ^{188}Bi^g in this work are reminiscent of a strongly coupled deformed band built on such a deformed configuration. Due to its large deformation, the moment of inertia of the band should be large, resulting in low-energy, strongly converted transitions. Typically, either $M1$, $E2$, or mixed $M1 + E2$ multipolarities are considered for the intraband transitions in such bands. Thus taking a 120-keV $M1$ or $E2$ transition as an example, the corresponding conversion coefficients are $\alpha_{tot}(120\,\text{keV}, M1) = 6.05$, $\alpha_K(120\,\text{keV}, M1) = 4.92$, $\alpha_{tot}(120\,\text{keV}, E2) = 3.14$, and $\alpha_K(120keV, E2) = 0.44$ [47], which indeed shows that the transition is strongly converted and can produce a large amount of $K_{\alpha,\beta}$ x rays. In other words, albeit tentatively, the observed prompt spectrum of γ rays and $K_{\alpha,\beta}$ x rays could provide an indirect confirmation of the strong deformation of ^{188}Bi^g.

To probe this possibility, the intensity balance between the prompt 102-, 127-, 153-, 165-, and 338-keV γ rays and the $K_{\alpha,\beta}$ x rays in Fig. 4(b) was also investigated. A range of 39%($E2$)–88%($M1$) for the expected $K_{\alpha,\beta}$ x-ray intensities

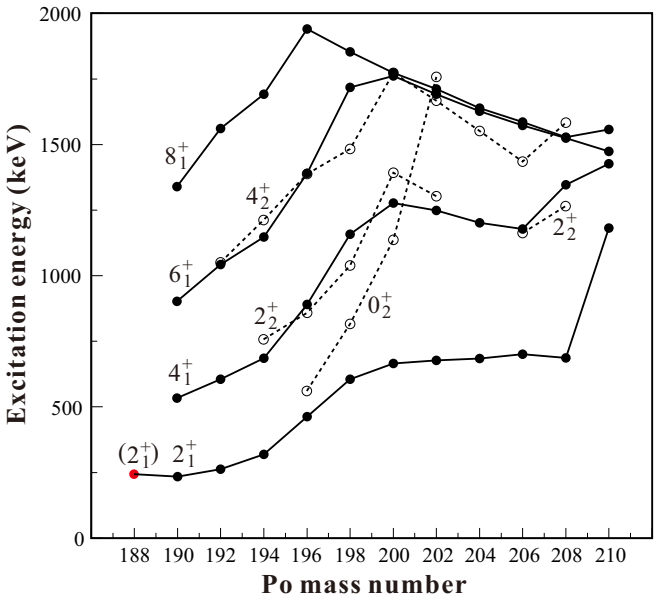

FIG. 10. Systematics of selected positive-parity near-yrast states for even-even polonium isotopes. Yrast states are indicated by filled circles. The non-yrast levels are indicated with empty circles. Tentative spin-parity assignment is given in parentheses. The data are taken from Refs. [13–18,48] and the present work (red symbol for ^{188}Po).

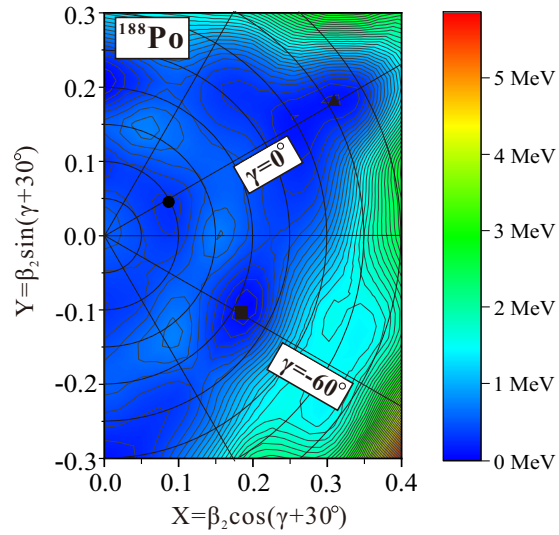

FIG. 11. PES for ^{188}Po. Nearly spherical, oblate, and prolate minima are indicated by the circle, square, and triangle, respectively. We made the energy at the lowest point of the PES be zero and the energy separation between the contour lines is 100 keV. The axis of oblate deformation lies at $\gamma = -60^\circ$ and that of prolate deformation at $\gamma = 0^\circ$.

relative to the observed ones was deduced, by applying either $E2$ or $M1$ for all of these transitions. Therefore, the number of $K_{\alpha,\beta}$ x rays could be quite well explained by the strong K conversion for the low-energy transitions of $M1/E2$ character, providing a justification for the presence of deformed rotational band.

C. ^{188}Po

Figure 10 shows the updated systematics of positive-parity yrast states up to 8_1^+ and near yrast states up to 4_2^+ for the even-mass $^{188-210}$Po isotopes, where we included our newest data for ^{188}Po. The fact that the new 242-keV transition in ^{188}Po smoothly extends the trend of the 2_1^+ states in the lightest Po isotopes was used to assign this transition as deexciting from this state.

As was mentioned in the Introduction, two different approaches have been used to interpret these systematics: an anharmonic quadrupole vibrator picture [15,17,19,20] and the intruder/shape coexistence framework with configuration mixing [13,14,18,21–26,50]. The most recent laser-spectroscopy data for $^{191-211}$Po isotopes [27,29] strongly support the shape coexistence scenario, which was extensively discussed in Ref. [30] and is briefly summarized below.

In the heavier polonium isotopes ($A \geqslant 198$), a dominant nearly spherical gs is present, which is confirmed by the measurements of the mean-square charge radii [12,27]. The oblate 0_2^+ bandhead is at a relatively high energy of ≈700 keV in ^{198}Po, thus no mixing with the gs is expected. As seen from the energies of the 0_2^+, 2_2^+ and 4_2^+ states in even-mass $^{194-198}$Po (Fig. 10), the oblate configuration descends in energy with decreasing neutron number, and mixing between the near spherical and oblate configurations is evident from the downward trend of the lowest states in even-A $^{192-198}$Po [26,30]. In addition, based on the calculated unperturbed spherical and oblate deformed 0^+ state energies in ^{192,194}Po [26], the oblate 0^+ state becomes the gs for ^{190,192}Po, with a close-lying nearly spherical 0^+ state. The latter conclusion was confirmed by PES calculations; see, e.g., Fig. 4 in Ref. [30] for ^{188,190,192}Po. Indeed, while two coexisting minima (weakly oblate and prolate) are seen in ^{192}Po, three close-lying minima were predicted for ^{188,190}Po (see Fig. 11), where we reproduce the PES for ^{188}Po. Based on these calculations, the prolate minimum is expected to become the gs in ^{188}Po, which was experimentally supported by the α-decay pattern of this nucleus; see extensive discussion in Refs. [30,32].

Therefore, three coexisting band structures are expected at low energy in ^{188}Po. Due to this, the positions of the lowest excited states, in particular of the 2_1^+ states in ^{188,190,192}Po, are expected to be strongly distorted by the mixing between two or even three bands. Therefore no clear inference on the nature of the 2_1^+ states in ^{188,190,192}Po can be made based on the energies.

D. The RDT efficiencies for different nuclei

In this section we return to the discussion of the dramatic difference between the *prompt* RDT spectra for ^{188}Bi^{g,m} and ^{186}Pb; see Fig. 4. To make it quantitative, we compare the RDT efficiency for these and several other nuclei produced in our experiment.

The RDT efficiency can be deduced as the ratio of the number of prompt γ rays from the RDT [γ(GS)-EVR]-α

TABLE I. The RDT γ-ray yields for prompt deexcitations for several lead and bismuth nuclides deduced in this experiment.

Nuclide	ε_{RDT}
^{186}Pb	52(6)%
^{188}Pb	44(4)%
^{187}Pb^{g}	21(4)[a]
^{187}Pb^{m}	15(3)[a]
^{189}Bi	16(3)%
^{188}Bi^{m}	(7–10)[b]

[a]The RDT spectra for ^{187}Pb^{g,m} were shown in Ref. [35]. To deduce the RDT efficiencies we considered the relevant transitions feeding to respective $3/2^-$ and $13/2^+$ states, and we avoided double counting of the γ rays within the respective bands.

[b]Only the intensity of the prompt 319-366-462-keV cascade was used for this estimation; if the intensity of the isomer deexcitation path is added, a lower limit of 17% would result for ^{188}Bi^{m}.

analysis to the number of respective EVR-α events, for a particular isotope. The number of observed γ decays must be corrected for the GS detection efficiency and internal conversion. Ideally, the level scheme itself should be well understood, to account for the probability of missing deexcitations which bypass the specific level from which the γ ray under investigation is emitted. The most suitable examples are typically provided by the level schemes of even-even isotopes, where the main deexcitation often proceeds via a dominant single yrast cascade, via the $2_1^+ \rightarrow 0_{gs}^+$ transition; e.g., via the 662-keV decay in ^{186}Pb [see Fig. 4(c)]. Taking ^{186}Pb as an example, we compare the number of the 6329-keV α decays in the time window of $\Delta T(\text{EVR} - 6329) < 20$ s in Fig. 1 with the corresponding number of the 662-keV γ rays in the RDT spectrum in Fig. 4(c), after correction with its GS efficiency and the $E2$ conversion. Based on this comparison, a value of $\varepsilon_{RDT}(^{186}\text{Pb}) = 52(6)\%$ was deduced assuming 100% of deexcitation goes via the 662-keV transition.

By using the same method, RDT efficiencies for other nuclei were derived as shown in Table I. We notice rather comparable values for the even-even isotopes ^{186,188}Pb, around 50%, which demonstrates an important intensity loss even for even-even nuclides.

A further RDT efficiency reduction by a factor of $\approx$2–3 is evident for the odd-mass isotopes ^{187}Pb^{g,m} and ^{189}Bi; this effect was already noticed in Ref. [51] for ^{187}Pb. Even a stronger reduction was deduced for the prompt cascade of γ-rays in ^{188}Bi^{m} in our study.

There are two possible reasons for the prompt RDT efficiency reduction.

(i) The presence of high-lying isomers with the half-lives of the order of 10–200 ns. Due to the recoil flight time of 600–800 ns through the separator, such isomers will not be seen by GS or by the focal plane detectors. Indeed, such isomers are known in, e.g., $^{188-206}$Pb [10,52]; they were studied by the so-called catcher technique with a pulsed beam.

(ii)Unobserved low-energy strongly converted γ-ray transitions. This effect can be clearly seen by comparing, e.g., the RDT spectra of ^{186}Pb and ^{188}Bi^{g,m} in Fig. 4, normalized to the same number of α decays. The intensities of $K_{\alpha,\beta}$ x rays are significantly different in the two spectra, being strong for ^{188}Bi^{g,m} while they are weak for ^{186}Pb. Indeed, the imbalance of intensity between the prompt γ rays and the $K_{\alpha,\beta}$ x rays for ^{188}Bi^{m} indicates the presence of unobserved low-energy strongly converted γ transitions, as inferred in Sec. IV A.

The above results on the RDT efficiencies are important for planning future experiments on these isotopes, as these phenomena may lead to a substantially lower γ statistics relative to rate estimates when these effects are not taken into account.

V. SUMMARY

The in-beam γ-ray spectroscopy of two nuclei, ^{188}Bi and ^{188}Po, in the vicinity of $N = 104$ midshell was performed with the GS Ge-detector array coupled to the AGFA gas-filled separator at ANL, meanwhile the delayed γ-ray spectroscopy of ^{188}Bi was performed with the X-Array at the focal plane. A new 0.25(5)-μs isomeric state and a prompt cascade were identified above the (10^-) α-decaying state in ^{188}Bi. A number of γ rays were also observed on top of ^{188}Bi^{g}. However, in both cases, no detailed level scheme could be proposed, due to the low γ-ray statistics collected. The strong reduction of the γ-ray intensities is especially dramatic for the strongly deformed $1^{(+)}$ state (^{188}Bi^{g}) and it was tentatively linked to the strong internal conversion within the presumably strongly deformed rotational band with many low-energy converted transitions built on top of this state. Therefore, this result tentatively and indirectly supports the conclusions from the recent laser-spectroscopy study at ISOLDE, where the large shape staggering between weakly deformed (10^-) and strongly deformed $1^{(+)}$ was proposed.

A 242-keV γ-ray transition in ^{188}Po was observed. Based on the level energy systematics and PES calculations, it has been tentatively assigned as the deexcitation of the predominantly prolate (2^+) state to the predominantly prolate 0^+ gs. To learn more on the intrinsic configurations of the ^{188}Po gs and excited states and the possible band structures, the extension of the level scheme to higher spin states and observation of non-yrast states would be necessary with improved Ge and separators, e.g., in terms of their respective efficiencies, better energy resolution for Ge array, and higher counting rate possibilities for Ge detectors and for DSSDs. Similar to heavier isotopes, where non-yrast band structures are known, the higher-lying, high-spin states should be less mixed, and thus could provide a clearer picture of the configurations involved.

The importance of considering the possible reduction of the RDT efficiency when planning in-beam experiments in this region of nuclei was also demonstrated.

ACKNOWLEDGMENTS

This work was supported by the Strategic Priority Research Program of Chinese Academy of Sciences (Grant No. XDB34000000), the National Key R&D Program of China (Contract No. 2018YFA0404402), the National Natural Science Foundation of China (Grants No. 12135004, No. 11635003, No. 11961141004, No. 11735017, and No.

U2032138). UK personnel are grateful for financial support from the STFC, and A.N.A. is partially funded by the Chinese Academy of Sciences President's International Fellowship Initiative (Grant No. 2020VMA0017). This work was supported by the U.S. Department of Energy, Office of Nuclear Physics, under Contract No. DE-AC02-06CH11357 and Grants No. DE-FG02-94ER41041 (UNC) and No. DE-FG02-97ER41033 (TUNL). This work was also supported by the Slovak Research and Development Agency (Contract No. APVV-18-0268) and Slovak Grant Agency VEGA (Project No. 1/0651/21). This research used resources of ANL's ATLAS facility, which is a DOE Office of Science User Facility. We thank the Target Labor team of GSI for preparing the targets for the experiment.

[1] K. Heyde and J. L. Wood, Rev. Mod. Phys. **83**, 1467 (2011).
[2] J. L. Wood and K. Heyde, J. Phys. G **43**, 020402 (2016).
[3] R. Julin, T. Grahn, J. Pakarinen, and P. Rahkila, J. Phys. G **43**, 024004 (2016).
[4] R. Julin, K. Helariutta, and M. Muikku, J. Phys. G **27**, R109 (2001).
[5] A. Barzakh, A. N. Andreyev, C. Raison, J. G. Cubiss, P. Van Duppen, S. Péru, S. Hilaire, S. Goriely, B. Andel, S. Antalic, M. Al Monthery, J. C. Berengut, J. Bieroń, M. L. Bissell, A. Borschevsky, K. Chrysalidis, T. E. Cocolios, T. Day Goodacre, J.-P. Dognon, M. Elantkowska *et al.*, Phys. Rev. Lett. **127**, 192501 (2021).
[6] G. Ulm, S. K. Bhattacherjee, P. Dabkiewicz, G. Huber, H.-J. Kluge, T. Kühl, H. Lochmann, E.-W. Otten, K. Wendt, S. A. Ahmad, W. Klempt, and R. Neugart, Z. Phys. A **325**, 247 (1986).
[7] B. A. Marsh, T. Day Goodacre, S. Sels, Y. Tsunoda, B. Andel, A. N. Andreyev, N. A. Althubiti, D. Atanasov, A. E. Barzakh, J. Billowes, K. Blaum, T. E. Cocolios, J. G. Cubiss, J. Dobaczewski, G. J. Farooq-Smith, D. V. Fedorov, V. N. Fedosseev, K. T. Flanagan, L. P. Gaffney, L. Ghys *et al.*, Nat. Phys. **14**, 1163 (2018).
[8] B. Andel, A. N. Andreyev, S. Antalic, M. Al Monthery, A. Barzakh, M. L. Bissell, K. Chrysalidis, T. E. Cocolios, J. G. Cubiss, T. Day Goodacre, N. Dubray, G. J. Farooq-Smith, D. V. Fedorov, V. N. Fedosseev, L. P. Gaffney, R. F. Garcia Ruiz, S. Goriely, C. Granados, R. D. Harding, R. Heinke *et al.*, Phys. Rev. C **102**, 014319 (2020).
[9] A. N. Andreyev, D. Ackermann, S. Antalic, H. J. Boardman, P. Cagarda, J. Gerl, F. P. Heßberger, S. Hofmann, M. Huyse, D. Karlgren, A. Keenan, H. Kettunen, A. Kleinböhl, B. Kindler, I. Kojouharov, A. Lavrentiev, C. D. O'Leary, M. Leino, B. Lommel, M. Matos *et al.*, Eur. Phys. J. A **18**, 39 (2003).
[10] F.G. Kondev, M. Wang, W.J. Huang, S. Naimi, and G. Audi, Chin. Phys. C **45**, 030001 (2021).
[11] A. N. Andreyev, S. Antalic, D. Ackermann, S. Franchoo, F. P. Heßberger, S. Hofmann, M. Huyse, I. Kojouharov, B. Kindler, P. Kuusiniemi, S. R. Lesher, B. Lommel, R. Mann, G. Münzenberg, K. Nishio, R. D. Page, J. J. Ressler, B. Streicher, S. Saro, B. Sulignano *et al.*, Phys. Rev. C **73**, 024317 (2006).
[12] D. Kowalewska, K. Bekk, S. Göring, A. Hanser, W. Kälber, G. Meisel, and H. Rebel, Phys. Rev. A **44**, R1442 (1991).
[13] K. Helariutta, J. F. C. Cocks, T. Enqvist, P. T. Greenlees, P. Jones, R. Julin, S. Juutinen, P. Jämsen, H. Kankaanpää, H. Kettunen, P. Kuusiniemi, M. Leino, M. Muikku, M. Piiparinen, P. Rahkila, A. Savelius, W. H. Trzaska, S. Törmänen, J. Uusitalo, R. G. Allatt *et al.*, Eur. Phys. J. A **6**, 289 (1999).
[14] D. Alber, R. Alfier, C. E. Bach, D. B. Fossan, H. Grawe, H. Kluge, M. Lach, K. H. Maier, M. Schramm, R. Schubart, M. P. Waring, L. Wood, H. Hübel, and J. Y. Zhang, Z. Phys. A **339**, 225 (1991).
[15] W. Younes, J. A. Cizewski, H. Q. Jin, L. A. Bernstein, D. P. McNabb, C. N. Davids, R. V. F. Janssens, T. L. Khoo, C. J. Lister, D. J. Blumenthal, M. P. Carpenter, D. Henderson, R. G. Henry, T. Lauritsen, D. T. Nisius, H. T. Penttilä, and M. W. Drigert, Phys. Rev. C **52**, R1723 (1995).
[16] K. Helariutta, T. Enqvist, P. Jones, R. Julin, S. Juutinen, P. Jämsen, H. Kankaanpää, P. Kuusiniemi, M. Leino, M. Muikku, M. Piiparinen, A. Savelius, W. H. Trzaska, S. Törmänen, J. Uusitalo, R. G. Allatt, P. A. Butler, P. T. Greenlees, and R. D. Page, Phys. Rev. C **54**, R2799 (1996).
[17] N. Fotiades, W. Younes, J. A. Cizewski, D. P. McNabb, K. Y. Ding, C. N. Davids, R. V. F. Janssens, D. Seweryniak, M. P. Carpenter, H. Amro, P. Decrock, P. Reiter, D. Nisius, L. T. Brown, S. Fischer, T. Lauritsen, J. Wauters, C. R. Bingham, M. Huyse, A. Andreyev *et al.*, Phys. Rev. C **55**, 1724 (1997).
[18] K. Van de Vel, A. N. Andreyev, R. D. Page, H. Kettunen, P. T. Greenlees, P. Jones, R. Julin, S. Juutinen, H. Kankaanpää, A. Keenan, P. Kuusiniemi, M. Leino, M. Muikku, P. Nieminen, P. Rahkila, J. Uusitalo, K. Eskola, A. Hürstel, M. Huyse, Y. Le Coz *et al.*, Eur. Phys. J. A **17**, 167 (2003).
[19] L. A. Bernstein, J. A. Cizewski, H.-Q. Jin, W. Younes, R. G. Henry, L. P. Farris, A. Charos, M. P. Carpenter, R. V. F. Janssens, T. L. Khoo, T. Lauritsen, I. G. Bearden, D. Ye, J. A. Becker, E. A. Henry, M. J. Brinkman, J. R. Hughes, A. Kuhnert, T. F. Wang, M. A. Stoyer *et al.*, Phys. Rev. C **52**, 621 (1995).
[20] W. Younes and J. A. Cizewski, Phys. Rev. C **55**, 1218 (1997).
[21] N. Bijnens, P. Decrock, S. Franchoo, M. Gaelens, M. Huyse, H. Y. Hwang, I. Reusen, J. Szerypo, J. von Schwarzenberg, J. Wauters, J. G. Correia, A. Jokinen, and P. Van Duppen, Phys. Rev. Lett. **75**, 4571 (1995).
[22] N. Bijnens, P. Decrock, S. Franchoo, M. Gaelens, M. Huyse, H.-Y. Hwang, I. Reusen, J. Szerypo, J. von Schwarzenberg, G. Vancraeynest, P. Van Duppen, and J. Wauters, Phys. Rev. C **58**, 754 (1998).
[23] J. Wauters, P. Dendooven, M. Huyse, G. Reusen, P. Lievens, P. Van Duppen, and the ISOLDE Collaboration, Z. Phys. A **344**, 29 (1992).
[24] J. Wauters, N. Bijnens, P. Dendooven, M. Huyse, H. Y. Hwang, G. Reusen, J. von Schwarzenberg, P. Van Duppen, R. Kirchner, and E. Roeckl, Phys. Rev. Lett. **72**, 1329 (1994).
[25] N. Bijnens, I. Ahmad, A. N. Andreyev, J. C. Batchelder, C. R. Bingham, D. Blumenthal, B. C. Busse, X. S. Chen, L. F. Conticchio, C. N. Davids, M. Huyse, R. V. F. Janssens, P. Mantica, H. Penttila, W. Reviol, D. Seweryniak, P. Van Duppen, W. B. Walters, J. Wauters, and B. E. Zimmerman, Z. Phys. A **356**, 3 (1996).
[26] A. Oros, K. Heyde, C. De Coster, B. Decroix, R. Wyss, B. Barrett, and P. Navratil, Nucl. Phys. A **645**, 107 (1999).

[27] T. E. Cocolios, W. Dexters, M. D. Seliverstov, A. N. Andreyev, S. Antalic, A. E. Barzakh, B. Bastin, J. Büscher, I. G. Darby, D. V. Fedorov, V. N. Fedosseyev, K. T. Flanagan, S. Franchoo, S. Fritzsche, G. Huber, M. Huyse, M. Keupers, U. Köster, Y. Kudryavtsev, E. Mané *et al.*, Phys. Rev. Lett. **106**, 052503 (2011).

[28] M. Seliverstov, T. Cocolios, W. Dexters, A. Andreyev, S. Antalic, A. Barzakh, B. Bastin, J. Büscher, I. Darby, D. Fedorov, V. Fedoseyev, K. Flanagan, S. Franchoo, S. Fritzsche, G. Huber, M. Huyse, M. Keupers, U. Köster, Y. Kudryavtsev, B. Marsh *et al.*, Phys. Lett. B **719**, 362 (2013).

[29] M. D. Seliverstov, T. E. Cocolios, W. Dexters, A. N. Andreyev, S. Antalic, A. E. Barzakh, B. Bastin, J. Büscher, I. G. Darby, D. V. Fedorov, V. N. Fedosseev, K. T. Flanagan, S. Franchoo, G. Huber, M. Huyse, M. Keupers, U. Köster, Y. Kudryavtsev, B. A. Marsh, P. L. Molkanov *et al.*, Phys. Rev. C **89**, 034323 (2014).

[30] K. Van de Vel, A. N. Andreyev, D. Ackermann, H. J. Boardman, P. Cagarda, J. Gerl, F. P. Heßberger, S. Hofmann, M. Huyse, D. Karlgren, I. Kojouharov, M. Leino, B. Lommel, G. Münzenberg, C. Moore, R. D. Page, S. Saro, P. Van Duppen, and R. Wyss, Phys. Rev. C **68**, 054311 (2003).

[31] A. N. Andreyev, S. Antalic, D. Ackermann, S. Franchoo, F. P. Heßberger, S. Hofmann, M. Huyse, I. Kojouharov, B. Kindler, P. Kuusiniemi, S. R. Lesher, B. Lommel, R. Mann, G. Münzenberg, K. Nishio, R. D. Page, J. J. Ressler, B. Streicher, S. Saro, B. Sulignano *et al.*, Phys. Rev. C **73**, 044324 (2006).

[32] P. Van Duppen and A. N. Andreyev, in *The Euroschool on Exotic Beams - Vol. 5*, edited by C. Scheidenberger and M. Pfützner (Springer, Cham, 2018), pp. 65–116.

[33] B. B. Back, EPJ Web Conf. **163**, 00003 (2017).

[34] A. N. Andreyev, D. Ackermann, P. Cagarda, J. Gerl, F. Heßberger, S. Hofmann, M. Huyse, A. Keenan, H. Kettunen, A. Kleinböhl, A. Lavrentiev, M. Leino, B. Lommel, M. Matos, G. Münzenberg, C. Moore, C. D. O'Leary, R. D. Page, S. Reshitko, S. Saro *et al.*, Eur. Phys. J. A **6**, 381 (1999).

[35] W. Zhang, A. Andreyev, Z. Liu, D. Seweryniak, H. Huang, Z. Li, J. Li, C. Guo, D. Doherty, A. Barzakh, P. Van Duppen, J. Cubiss, B. Andel, S. Antalic, M. Block, A. Bronis, M. Carpenter, P. Copp, B. Ding, Z. Favier *et al.*, Phys. Lett. B **829**, 137129 (2022).

[36] H. Huang *et al.*, Phys. Lett. B **833**, 137345 (2022).

[37] A. J. Mitchell, P. F. Bertone, B. DiGiovine, C. J. Lister, M. P. Carpenter, P. Chowdhury, J. A. Clark, N. D'Olympia, A. Y. Deo, F. G. Kondev, E. A. McCutchan, J. Rohrer, G. Savard, D. Seweryniak, and S. Zhu, Nucl. Instrum. Methods Phys. Res., Sect. A **763**, 232 (2014).

[38] I. Y. Lee, Nucl. Phys. A **520**, c641 (1990).

[39] E. S. Paul, P. J. Woods, T. Davinson, R. D. Page, P. J. Sellin, C. W. Beausang, R. M. Clark, R. A. Cunningham, S. A. Forbes, D. B. Fossan, A. Gizon, J. Gizon, K. Hauschild, I. M. Hibbert, A. N. James, D. R. LaFosse, I. Lazarus, H. Schnare, J. Simpson, R. Wadsworth *et al.*, Phys. Rev. C **51**, 78 (1995).

[40] R. S. Simon, K.-H. Schmidt, F. P. Heßberger, S. Hlavac, M. Honusek, G. Münzenberg, H.-G. Clerc, U. Gollerthan, and W. Schwab, Z. Phys. A **325**, 197 (1986).

[41] P. Misaelides, P. Tidemand-Petersson, U. J. Schrewe, I. S. Grant, R. Kirchner, O. Klepper, I. C. Malcolm, P. J. Nolan, E. Roeckl, W.-D. Schmidt-Ott, and J. L. Wood, Z. Phys. A **301**, 199 (1981).

[42] W.J. Huang, M. Wang, F.G. Kondev, G. Audi, and S. Naimi, Chin. Phys. C **45**, 030002 (2021).

[43] A. Hürstel, M. Rejmund, E. Bouchez, P. T. Greenlees, K. Hauschild, S. Juutinen, H. Kettunen, W. Korten, Y. Le Coz, P. Nieminen, C. Theisen, A. N. Andreyev, F. Becker, T. Enqvist, P. M. Jones, R. Julin, H. Kankaanpää, A. Keenan, P. Kuusiniemi, M. Leino *et al.*, Eur. Phys. J. A **15**, 329 (2002).

[44] G. Audi, F. G. Kondev, M. Wang, W. Huang, and S. Naimi, Chin. Phys. C **41**, 030001 (2017).

[45] A. Hürstel, Y. Le Coz, E. Bouchez, A. Chatillon, A. Görgen, P. T. Greenlees, K. Hauschild, S. Juutinen, H. Kettunen, W. Korten, P. Nieminen, M. Rejmund, C. Theisen, J. Wilson, A. N. Andreyev, F. Becker, T. Enqvist, P. M. Jones, R. Julin, H. Kankaanpää *et al.*, Eur. Phys. J. A **21**, 365 (2004).

[46] A. N. Andreyev, M. Huyse, P. Van Duppen, J. F. C. Cocks, K. Helariutta, H. Kettunen, P. Kuusiniemi, M. Leino, W. H. Trzaska, K. Eskola, and R. Wyss, Phys. Rev. Lett. **82**, 1819 (1999).

[47] T. Kibédi, T. W. Burrows, M. B. Trzhaskovskaya, P. M. Davidson, and C. W. Nestor, Nucl. Instrum. Methods Phys. Res., Sect. A **589**, 202 (2008).

[48] R. B. Firestone and V. S. Shirley, *Table of Isotopes, 2 Volume Set,* 8th edition (Wiley-Interscience, New York, 1998), p. 3168.

[49] M. Huyse, E. Coenen, K. Deneffe, P. van Duppen, K. Heyde, and J. van Maldeghem, Phys. Lett. B **201**, 293 (1988).

[50] B. Andel, A. N. Andreyev, S. Antalic, F. P. Heßberger, D. Ackermann, S. Hofmann, M. Huyse, Z. Kalaninová, B. Kindler, I. Kojouharov, P. Kuusiniemi, B. Lommel, K. Nishio, R. D. Page, B. Sulignano, and P. Van Duppen, Phys. Rev. C **93**, 064316 (2016).

[51] A. M. Baxter, A. P. Byrne, G. D. Dracoulis, P. M. Davidson, T. R. McGoram, P. H. Regan, C. Chandler, W. Gelletly, C. Wheldon, R. Julin, J. F. C. Cocks, K. Helariutta, P. Jones, S. Juutinen, H. Kankaanpää, H. Kettunen, P. Kuusiniemi, M. Leino, M. Muikku, A. Savelius *et al.*, Phys. Rev. C **58**, 2671 (1998).

[52] G. D. Dracoulis, A. P. Byrne, A. M. Baxter, P. M. Davidson, T. Kibédi, T. R. McGoram, R. A. Bark, and S. M. Mullins, Phys. Rev. C **60**, 014303 (1999).